

# Trends in the extremes of environments associated with severe US thunderstorms

Erwan Koch<sup>\*</sup>, Jonathan Koh<sup>†</sup>, Anthony C. Davison<sup>‡</sup>  
Chiara Lepore<sup>§</sup>, Michael K. Tippett<sup>¶</sup>

January 30, 2019

## Abstract

Severe thunderstorms can have devastating impacts. Concurrently high values of Convective Potential Energy (CAPE) and Storm Relative Helicity (SRH) are known to be favourable to severe weather, so we consider their extreme values for a large area of the contiguous US over the period 1979–2015. We use extreme-value theory and a multiple testing procedure to show that there is a significant time trend in the extremes for CAPE maxima in April, May and June, for SRH maxima in May, and for maxima of  $\text{PROD} = \sqrt{\text{CAPE}} \times \text{SRH}$  in April, May and August. Moreover, we show that the El Niño-Southern Oscillation explains variation in the extremes of PROD and SRH in February. Our results imply that the risk of severe thunderstorms in April and May tends to increase in parts of the US where this risk was already high and that the storm risk in February tends to be higher over the main part of the region during La Niña years.

## 1 Introduction

Annual losses from severe thunderstorms in the US have exceeded \$10 billion in recent years.<sup>1</sup> In addition to economic losses, 2011 was marked by 552 deaths caused by tornadoes. These economic and human impacts are a strong motivation for the study of how and why US thunderstorm activity varies from year to year and region to region. Two important aspects of the variability of thunderstorm activity are trends, potentially related to climate change or multi-decadal variability, and modulation by the El Niño-Southern

---

<sup>\*</sup>Institute of Mathematics, EPFL, Station 8, 1015 Lausanne, Switzerland.  
Email: erwan.koch@epfl.ch

<sup>†</sup>Institute of Mathematics, EPFL, Station 8, 1015 Lausanne, Switzerland.  
Email: jonathan.koh@epfl.ch

<sup>‡</sup>Institute of Mathematics, EPFL, Station 8, 1015 Lausanne, Switzerland.  
Email: anthony.davison@epfl.ch

<sup>§</sup>Lamont-Doherty Earth Observatory, Columbia University, Palisades, New York, USA.  
Email: clepore@ldeo.columbia.edu

<sup>¶</sup>Department of Applied Physics and Applied Mathematics, Columbia University, New York, New York, USA.  
Email: mkt14@columbia.edu

<sup>1</sup>[http://www.willisre.com/Media\\_Room/Press\\_Releases\\_\(Browse\\_All\)/2017/WillisRe\\_Impact\\_of\\_ENSO\\_on\\_US\\_Tornado\\_and\\_Hail\\_frequencies\\_Final.pdf](http://www.willisre.com/Media_Room/Press_Releases_(Browse_All)/2017/WillisRe_Impact_of_ENSO_on_US_Tornado_and_Hail_frequencies_Final.pdf)

Oscillation (ENSO). However, inadequacies in the length and quality of the thunderstorm data record present substantial challenges to addressing these questions directly (Verbout et al., 2006; Allen and Tippett, 2015; Edwards et al., 2018).

Several recent studies have analyzed trends in US tornado reports and have found that annual numbers of reliably observed tornadoes, i.e., those rated E/EF1 and greater, show slight downward but statistically insignificant trends over time (Brooks et al., 2014; Elsner et al., 2015). On the other hand, measures of tornado outbreaks or clusters show upward trends (Brooks et al., 2014; Elsner et al., 2015; Tippett et al., 2016). Changes in regional tornado activity have also been reported (Agee et al., 2016; Gensini and Brooks, 2018). There is less evidence for changes in hail and damaging straight-line wind, perhaps due to the poorer quality of the relevant databases.

Given the limitations of the historical storm record, analysis of meteorological environments that are associated with severe thunderstorms is a practical alternative approach. Environments that are favourable to severe thunderstorms, especially supercell storms, include convective available potential energy (CAPE) and vertical wind shear (see, e.g., Brooks et al., 2003; Brooks, 2013). Various measures of vertical wind shear have been used for this purpose, including storm relative helicity (SRH). Since the 1990s, weather forecasters have routinely used such quantities as part of the forecast process to interpret observations and numerical weather prediction model output (Davies et al., 1993; Rasmussen and Blanchard, 1998; Doswell et al., 1996). Later the same approach was effective in climatological studies, especially in areas outside the US without extensive historical reports (Brooks et al., 2003). Likewise, the environmental approach can provide an indication of expected severe thunderstorm activity in a warmer climate based on climate projections that do not resolve thunderstorms explicitly (Trapp et al., 2009; Diffenbaugh et al., 2013). On time-scales between weather forecasts and climate projections, this approach has provided a clearer picture of how ENSO modulates US hail and tornado activity (Allen et al., 2015; Lepore et al., 2017).

However, there are notable gaps in previous statistical studies of environments associated with severe thunderstorms. For instance, relationships with ENSO were diagnosed based on *monthly* averages, a quantity that is at best an indirect proxy for behaviour on the time-scale of weather. Similarly Gensini and Brooks (2018) computed monthly accumulations of daily maxima of a significant tornado parameter. Tippett et al. (2016) used submonthly environmental data but aggregated the results on an annual and US-wide basis. These gaps motivate the present work, which focuses on extremes of the environmental values rather than monthly means, and presents results that are spatially and temporally resolved. The framework that we use is statistical extreme-value theory.

Using extreme-value theory, Mannshardt and Gilleland (2013) study the annual maxima of the variable  $WS \times W_{\max}$ , where  $WS$  is a measure of wind shear and  $W_{\max} = \sqrt{2 \times \text{CAPE}}$ . They show the existence of a time trend in the location parameter of a fitted generalized extreme-value (GEV) distribution but do not investigate whether this trend is due to both CAPE and  $WS$  or only to one of these variables. Moreover, they study yearly maxima and thus cannot detect interesting month-specific features, and they do not account for multiple testing, though this is briefly addressed in Gilleland et al. (2008). Finally, they consider only time as a covariate.

We propose to overcome at least some of the shortcomings of the previously mentioned paper. Our study covers a large part of the US for individual months from 1979 to 2015. We separately consider CAPE, SRH and the combined variable  $\text{PROD} = \sqrt{\text{CAPE}} \times \text{SRH}$ . We carefully check the relevance of the GEV and the use of explanatory variables in the

location parameter of the GEV, and we allow for multiple testing by implementing the false discovery rate procedure of Benjamini and Hochberg (1995). Finally, we consider ENSO as a covariate in the location parameter of the GEV, and show the existence of a significant trend for PROD maxima in April, May and August (and to a lesser extent in June and December), CAPE maxima in April, May and June (and to a lesser extent in August, November and January) and SRH maxima in May (and to a lesser extent in April). April and May are important months for PROD, as severe thunderstorms are frequent at this period. The corresponding time slope is positive in already risky regions of the US, which may have important impact in terms of risk assessment and management. In addition, our study reveals that ENSO can explain variation in the location parameter of the GEV for PROD and SRH maxima in February. The corresponding slope for SRH is negative over most of the region we consider, possibly suggesting an increase of storm risk in February during La Niña years.

The remainder of the paper is organized as follows. Section 2 presents the data and a brief exploratory analysis. We describe our modelling and testing strategy and demonstrate its relevance in Section 3. Section 4 details our main results. Section 5 contains a summary and discussion of our findings.

## 2 Data

The data we investigate consist of 3-hourly time-series of 0-180 hPa convective potential energy (CAPE,  $\text{Jkg}^{-1}$ ) and 0-3 km storm relative helicity (SRH,  $\text{m}^2\text{s}^{-2}$ ) from 1 January 1979 at 00:00 to 31 December 2015 at 21:00. The region covered is a rectangle over the contiguous US from  $-110^\circ$  to  $-80^\circ$  longitude and  $30^\circ$  to  $50^\circ$  latitude and the resolution is  $1^\circ$  longitude and  $1^\circ$  latitude. These data constitute a coarse version of reanalysis data from the North American Regional Reanalysis (NARR); the original resolution is 32km longitude and 32km latitude (see, e.g., Mesinger and Coauthors, 2006). The region contains 651 grid points, with no data available for 32 grid points over the sea or lakes. Using these time series, we build 3-hourly times series of  $\text{PROD} = \sqrt{\text{CAPE}} \times \text{SRH}$ , measured in  $\text{m}^3\text{s}^{-3}$ , which is highly representative of the risk of severe thunderstorms (see, e.g., Brooks et al., 2003, especially Figure 1 and Equation (1)).

As a physical covariate we use monthly values of the NINO 3.4 index ( $^\circ\text{C}$ ) from 1979 to 2015, taken from the ERSSTv5 data set available on the NOAA Climate Prediction Center website.

Figure 1 shows the empirical pointwise probabilities that CAPE and SRH exceed thresholds corresponding to roughly the 90<sup>th</sup> percentile of each variable across the entire region. There is a clear North-South gradient for CAPE probabilities, while the regional spatial pattern for SRH suggests that the high values cluster towards the centre of the region.

Figure 2 shows an increase in the exceedance probabilities for PROD at many grid points over the decades; a similar result is visible for SRH, but less so for CAPE. This increase is of interest for risk assessment, especially in regions where the risk of severe thunderstorms is high. Figure 2 strongly suggests a need to incorporate a temporal trend into our statistical modelling of maxima.

The top left panel of Figure 3 shows a positive correlation between PROD April maxima and time for many grid points, and the middle panels show a positive linear time trend for April maxima of PROD, CAPE and SRH in the subregion indicated. The

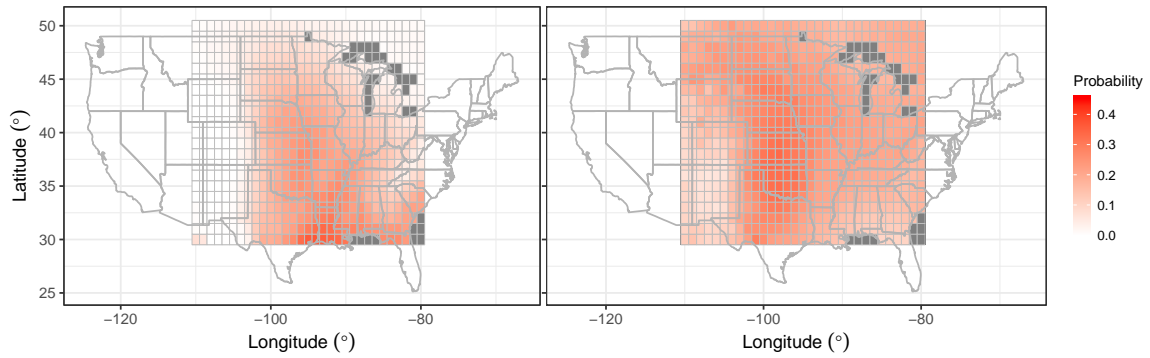


Figure 1: Empirical pointwise probabilities of 3-hourly CAPE exceeding  $1400\text{Jkg}^{-1}$  (left) and SRH exceeding  $170\text{m}^2\text{s}^{-2}$  (right) for the entire period 1979–2015. Dark grey corresponds to grid points where no observations are available.

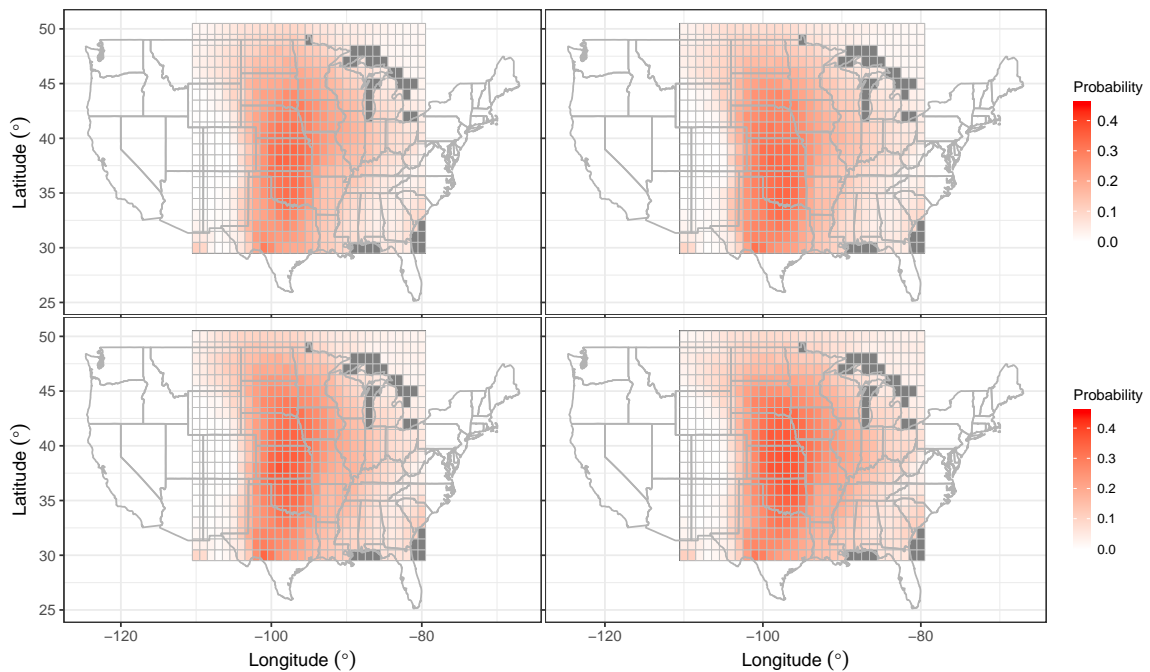


Figure 2: Empirical pointwise probabilities of 3-hourly PROD exceeding  $3300\text{m}^3\text{s}^{-3}$  during the periods 1979–1987 (top left), 1988–1996 (top right), 1997–2005 (bottom left) and 2006–2015 (bottom right).

top right panel shows strong negative correlation between PROD February maxima and ENSO at many grid points, while the scatter-plots in the bottom panel show a roughly linear negative trend for all variables. These analyses underscore the need to incorporate ENSO into our statistical modelling of maxima.

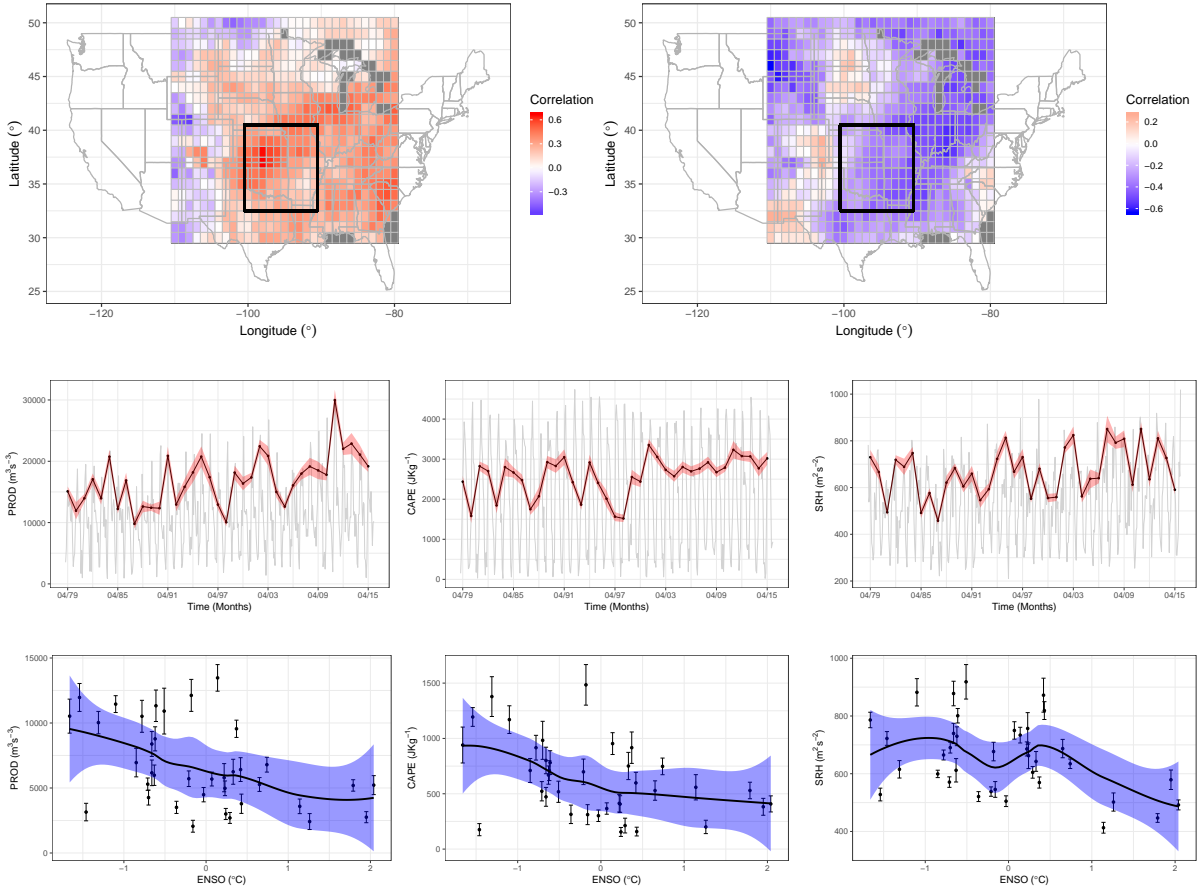


Figure 3: Exploratory analysis for monthly maxima: The top panels show the correlation map with time (in years from 1 to 37) for PROD April maxima (left) and the correlation map with ENSO for PROD February maxima (right). The middle and bottom panels display PROD (left), CAPE (centre) and SRH (right) analyses on a subregion indicated by the black rectangle drawn on the correlation maps. The middle panels show the region-averaged monthly maxima time series across all 444 months in light grey, the region-averaged April maxima time series in black and its 95% confidence interval bounds indicated by the red shaded region. Every point in the time series is the averaged maxima across all grid points in the subregion indicated before, for a particular month and a particular year. The bottom panels show scatter-plots of the region-averaged February maxima with ENSO, along with the 95% confidence interval bounds at each point indicated by the whiskers. The black line represents the best fitted local regression trend estimate, with its 95% confidence interval bounds indicated by the shaded blue region.

## 3 Methodology

### 3.1 Modelling of maxima

Risk assessment entails the estimation of return levels associated with very high return periods and of the probabilities of observing events so extreme that they have never occurred before. Extreme-value theory provides a solid framework for the extrapolation needed to perform these tasks for the maxima of PROD, CAPE and SRH. Here we present the statistical background underpinning the results in Section 4; for further explanation and references see Coles (2001) or Davison and Huser (2015).

Let  $M_n$  denote the maximum of the independent and identically distributed random variables  $X_1, \dots, X_n$ . The extremal types theorem states that if there exist sequences  $\{a_n\} > 0$  and  $\{b_n\} \in \mathbb{R}$  such that  $(M_n - b_n)/a_n$  has a non-degenerate limiting distribution as  $n \rightarrow \infty$ , then this must be a generalized extreme-value (GEV) distribution,

$$\text{GEV}_{\eta, \tau, \xi}(x) = \begin{cases} \exp \left[ - \{1 + \xi(x - \eta)/\tau\}_+^{-1/\xi} \right], & \xi \neq 0, \\ \exp \left[ - \exp \{-(x - \eta)/\tau\}_+ \right], & \xi = 0, \end{cases} \quad x \in \mathbb{R}, \quad (1)$$

where  $\xi$  and  $\eta$  are real-valued,  $\tau > 0$  and, for any real  $a$ ,  $a_+ = \max\{a, 0\}$ . This implies that if  $n$  is large enough, we may approximate the distribution of  $M_n$  by

$$\mathbb{P}(M_n \leq x) \approx \text{GEV}_{\eta, \tau, \xi}(x), \quad x \in \mathbb{R}, \quad (2)$$

for suitably chosen  $\eta$ ,  $\tau$  and  $\xi$ . The parameters  $\eta$ ,  $\tau$  and  $\xi$  are the location, scale and shape parameters. The shape parameter  $\xi$  defines the type of the distribution:  $\xi > 0$ ,  $\xi < 0$  and  $\xi = 0$  correspond to the Fréchet, Weibull and Gumbel types and can encompass quite different statistical behaviours, with the first giving a heavy upper tail with polynomial decay, the second modelling bounded variables, and the third an intermediate case, unbounded but with an exponentially-decaying upper tail.

The GEV approximation for maxima remains valid if the variables are dependent, provided that distant extremes are “nearly independent” (more formally, that Leadbetter’s  $D(u_n)$  condition is satisfied). We shall see below that this appears to be the case for our time series, so (2) applies.

The results above provide a natural model for maxima of stationary sequences. To apply this model we split the data into blocks of equal lengths and compute the maximum of each block. Assume that we have  $T$  blocks of length  $n$  and let  $M_n^{(1)}, \dots, M_n^{(T)}$  denote the corresponding maxima. If  $n$  is large enough, the distribution of the  $M_n^{(t)}$  is approximately (2), upon which inference can be based; this is the so-called block maximum method. As noted in Section 2, PROD, CAPE and SRH maxima exhibit a time trend and/or a relation with ENSO for some months, and then we can allow the GEV parameters to depend upon these variables. Figure 4 and results in Section 4 show that the temporal or ENSO effects only appear for certain months. For instance, time trends for PROD, CAPE and SRH are mainly present in April and May, April to June and April and May, respectively. We therefore choose our blocks to be the months and study each month separately, fitting the models

$$M_n^{(t)} \sim \text{GEV}_{\eta_{\text{ti}}(t), \tau_{\text{ti}}, \xi_{\text{ti}}}, \quad \eta_{\text{ti}}(t) = \eta_{0, \text{ti}} + \eta_{1, \text{ti}} t, \quad t = 1, \dots, T, \quad (3)$$

and

$$M_n^{(t)} \sim \text{GEV}_{\eta_{\text{en}}(t), \tau_{\text{en}}, \xi_{\text{en}}}, \quad \eta_{\text{en}}(t) = \eta_{0, \text{en}} + \eta_{1, \text{en}} \text{ENSO}_t, \quad t = 1, \dots, T, \quad (4)$$

where  $\eta_{0, \text{ti}}$ ,  $\eta_{1, \text{ti}}$ ,  $\eta_{0, \text{en}}$ ,  $\eta_{1, \text{en}}$ ,  $\xi_{\text{ti}}$  and  $\xi_{\text{en}}$  are real-valued,  $\tau_{\text{ti}}$  and  $\tau_{\text{en}}$  are positive,  $\text{ENSO}_t$  is the value of ENSO in that month for year  $t$ , and  $n$  equals 224, 232, 240 or 248, depending on the number of days in the month, as we have eight observations per day. Figure 3 suggests that effects of time and ENSO on maxima are roughly linear and impact the location parameter  $\eta$  only, so we consider constant scale and shape parameters; it is generally inappropriate to allow the latter depend on a covariate owing to the large uncertainty of its estimate. The time trend induces non-stationarity between the blocks (i.e., across

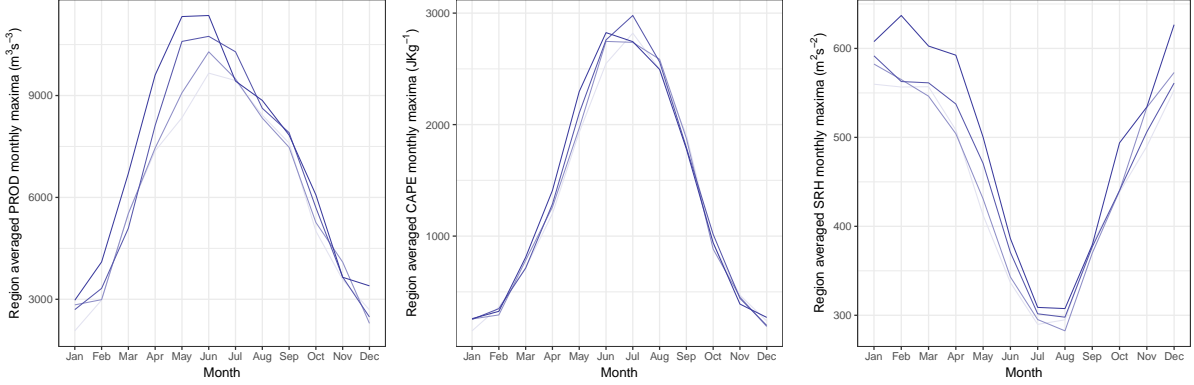


Figure 4: Whole region-averaged monthly maxima of PROD (left), CAPE (centre) and SRH (right). The four lines coloured from light blue to dark blue correspond to the time periods 1979–1987, 1988–1996, 1997–2005 and 2006–2015, respectively.

years) but does not violate the within-block stationarity assumption; see below. Figure 4 suggests that the time trend does not stem from a shift of seasonality.

We compute the monthly maximum for each month and a given grid point and thereby obtain the maxima  $M_{31}^{(1)}, \dots, M_{31}^{(37)}$  for January, say. We then fit the models (3) and (4) by numerical maximum likelihood estimation for each month and grid point.

Recall that within-block stationarity and the  $D(u_n)$  condition ensure the validity of (2) and hence allow us to consider the models (3) and (4). To check the plausibility of these two properties, we considered the 3-hourly time series of PROD, CAPE and SRH at 50 representative grid points. For each block (associated with a triplet grid point-month-year), we fitted several autoregressive-moving average (ARMA) processes to the corresponding time series, chose the fit that minimised the Akaike information criterion (AIC), and used a Box–Pierce procedure to assess the independence of the corresponding residuals; we found no systematic departure from independence or stationarity. Often the residual distribution appeared to lie in the Fréchet or Gumbel maximum-domains of attraction, and Embrechts et al. (1997, §5.5) show that in such cases convergence of the maxima to the GEV occurs even for ARMA processes; this is related to the  $D(u_n)$  condition. Hence the time series of data within the months seem to satisfy both stationarity and the  $D(u_n)$  condition. Choosing the months as blocks thus appears reasonable, as is confirmed by our analysis in Section 3.2. The need for within-block stationarity rules out years or seasons, owing to the clear seasonality appearing in Figure 4, while blocks equivalent to years or seasons would mask many interesting features. Finally, the sample size associated with days and weeks is too low for the GEV approximation (2) to be reasonable.

### 3.2 Assessment of GEV fit

At each grid point  $i$  and month  $j$ , we fit the GEV to the monthly maxima, as described in Section 3.1, resulting in location, scale and shape parameter estimates  $\hat{\eta}_{i,j}$ ,  $\hat{\tau}_{i,j}$  and  $\hat{\xi}_{i,j}$ . We use the Kolmogorov–Smirnov test to assess the distributional proximity between this GEV and the empirical distribution of the 37 observed monthly maxima. For PROD, CAPE and SRH, in most months, the fit appears acceptable at all grid points at the 5% level. These good in-sample fits of the GEV for all variables are confirmed by the quantile-quantile (QQ) plots, which are displayed for one grid point in Figure 5.

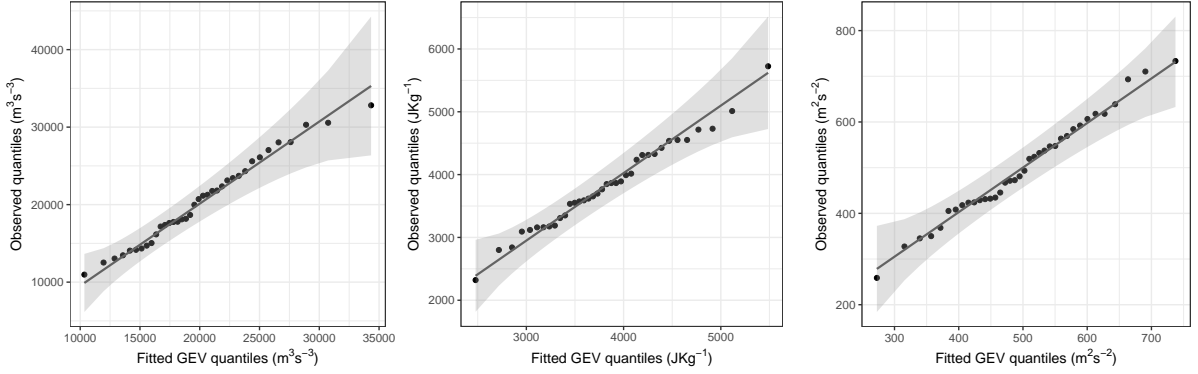


Figure 5: Assessment of the in-sample fit of the GEV: QQ plots for PROD (left), CAPE (centre) and SRH (right) May maxima at the grid point whose South-West corner has coordinates  $32^\circ$  latitude and  $-99^\circ$  longitude. The shaded regions indicate the 95% confidence bounds.

However, these results do not take into account the fitting of the GEV to the data, which systematically decreases the values of the Kolmogorov–Smirnov statistic. In order to make an informal allowance for this, we perform the following procedure for each grid point  $i$  and month  $j$ :

1. fit the GEV using the pooled observations from the eight grid points nearest to  $i$  to obtain  $\hat{\eta}_{\text{po}_i,j}$ ,  $\hat{\tau}_{\text{po}_i,j}$  and  $\hat{\xi}_{\text{po}_i,j}$ ;
2. use a Kolmogorov–Smirnov test to check the agreement between the “out-sample” GEV with parameters  $\hat{\eta}_{\text{po}_i,j}$ ,  $\hat{\tau}_{\text{po}_i,j}$  and  $\hat{\xi}_{\text{po}_i,j}$ , and the empirical distribution of the 37 observed monthly maxima.

Then, we implement the same procedure 100 times with data simulated from the GEV fitted at each grid point and compute the mean number of rejections. We only show corresponding results for SRH, as those for PROD and CAPE are similar. Table 1 shows that the numbers of rejections for all variables are comparable with those obtained in the simulation study (accounting for variability) or slightly higher. This procedure supports the use of the GEV at grid points at which no data are available. We conclude that the

| Variable          | Jan | Feb | Mar | Apr | May | Jun | Jul | Aug | Sep | Oct | Nov | Dec |
|-------------------|-----|-----|-----|-----|-----|-----|-----|-----|-----|-----|-----|-----|
| <b>PROD</b>       | 50  | 37  | 78  | 32  | 51  | 61  | 70  | 73  | 56  | 32  | 43  | 39  |
| <b>CAPE</b>       | 67  | 41  | 56  | 40  | 61  | 66  | 71  | 92  | 68  | 43  | 61  | 77  |
| <b>SRH</b>        | 36  | 23  | 24  | 21  | 22  | 42  | 42  | 34  | 35  | 26  | 24  | 36  |
| <b>Simulation</b> | 44  | 44  | 46  | 42  | 44  | 51  | 45  | 43  | 48  | 49  | 46  | 46  |

Table 1: Assessment of the out-sample fit of the GEV: Number of rejections from our out-sample Kolmogorov–Smirnov test for each month and each variable. The last row gives the average number of rejections when performing the simulation study.

GEV provides a suitable model for the monthly maxima of our three variables.



### 3.3 Testing procedure

#### 3.3.1 General

In Section 4, we assess whether time and ENSO affect the location parameter of the fitted GEV for the three variables PROD, CAPE and SRH. However, as this is assessed at 619 grid points, we must make some allowance for multiple hypothesis testing.

We first discuss the statistic used to test the significance of time and ENSO, respectively, in (3) and (4). In the first case, we have to test the null hypothesis

$$H_0 : \eta_{1,ti} = 0 \quad \text{versus} \quad H_A : \eta_{1,ti} \neq 0,$$

by comparing the fits of the models

$$\mathcal{M}_0 : \eta_{ti}(t) = \eta_{0,ti}, \quad \mathcal{M}_1 : \eta_{ti}(t) = \eta_{0,ti} + \eta_{1,ti}t, \quad t = 1, \dots, 37,$$

and similarly for ENSO. We let  $\ell_0(\mathcal{M}_0)$  and  $\ell_1(\mathcal{M}_1)$  denote the maximized log-likelihoods for the models  $\mathcal{M}_0$  and  $\mathcal{M}_1$  and compute the signed likelihood ratio statistic  $\tilde{T} = \text{sgn}(\hat{\eta}_{1,ti})[2\{\ell_1(\mathcal{M}_1) - \ell_0(\mathcal{M}_0)\}]^{1/2}$ , where  $\text{sgn}(\hat{\eta}_{1,ti})$  is the sign of the estimated trend under model  $\mathcal{M}_1$ ;  $\tilde{T}$  has an approximate standard Gaussian distribution under  $H_0$ , and the corresponding  $p$ -value is  $p = 2\Phi(-|\tilde{t}|)$ , where  $\tilde{t}$  is the observed value of  $\tilde{T}$  and  $\Phi$  denotes the standard Gaussian distribution function. Computing  $p$  for the  $m$  grid points yields  $m$  ordered  $p$ -values  $p_{(1)} \leq p_{(2)} \leq \dots \leq p_{(m)}$ . The underlying  $p$ -values are likely to be positively correlated, since dependence on time or ENSO will have a spatial component, and we now discuss how to adjust for this.

#### 3.3.2 Multiple testing

A popular approach for multiple testing in climatology is the field significance test of Livezey and Chen (1983), but unfortunately this gives little insight about where the results are significant, which is of high interest to us, and the regression approach of Del-Sole and Yang (2011) has the same drawback. Among methods to identify grid points where the results are significant are those, such as the Bonferroni method, that strongly control the so-called family-wise error rate, i.e., the probability that the number of falsely rejected null hypotheses is equal or larger than unity. However, when the number of hypotheses to test is high, such methods are so stringent that the power of the test is very low.

Benjamini and Hochberg (1995) introduce the false discovery rate (FDR), namely the expected proportion of false rejections of the null hypothesis  $H_0$  out of all rejections of it, and propose a procedure to ensure that the FDR is less than a given level  $q$  when performing multiple testing. Their approach, which we call the BH procedure, would reject  $H_0$  at all grid points  $i$  such that  $p_i \leq p_{(k)}$ , where

$$k = \max \left\{ i : p_{(i)} \leq q \frac{i}{m} \right\}.$$

In fact this ensures that the FDR is less than  $qm_0/m$ , where  $m_0$  denotes the unknown number of grid points at which  $H_0$  is true. We then say that the procedure controls the false discovery rate at level  $qm_0/m$ .

For a chosen  $q$ , let  $S_q$  be the number of grid points at which a particular covariate is declared significant by the BH procedure. Then we expect the true number of grid points where the relation is significant,  $m_A$ , to satisfy

$$m_A \geq (1 - q)S_q. \quad (5)$$

As the BH procedure ensures that the false discovery rate is not more than  $qm_0/m$ , we may argue a posteriori that we have controlled the FDR at level

$$q^{(1)} = \frac{q\{m - (1 - q)S_q\}}{m} \leq q \frac{m_0}{m},$$

which entails that  $m_A \geq (1 - q^{(1)})S_q$ . Iterating this argument by defining

$$q^{(n+1)} = \frac{q\{m - (1 - q^{(n)})S_q\}}{m}, \quad n = 1, 2, \dots,$$

the effective level at which we have controlled the FDR is therefore  $q_{\text{lim}} = \lim_{n \rightarrow \infty} q^{(n)}$ . This limit is generally obtained after a few iterations. Finally, we may write that

$$m_A \geq (1 - q_{\text{lim}})S_q. \quad (6)$$

The BH procedure was originally shown to be valid for independent test statistics, but Benjamini and Yekutieli (2001, Theorem 2.1) prove that it controls the FDR at level  $qm_0/m$  if the statistics have a certain form of positive dependence. Ventura et al. (2004) apply the BH procedure to simulations representative of climatological data and covering the range of correlation scales likely to be encountered in practice, and find that it controls the FDR at level  $qm_0/m$ . Yekutieli and Benjamini (1999) and Benjamini and Yekutieli (2001) propose modifications to account for more general dependence between the test statistics. The first is complicated and its gain over the BH procedure is limited, while the second is applicable whatever the dependence structure but has greatly reduced power, so Ventura et al. (2004) recommend the use of the BH procedure.

The independence assumption underlying the BH procedure is clearly false for our data, but since they are climatological, they should be close enough to those considered in Ventura et al. (2004) and so applying the BH procedure at level  $q$  should control the FDR at level  $qm_0/m$ . A more rigorous argument would use the asymptotic normality of our test statistic  $\tilde{T}$  and the multivariate central limit theorem to show that  $\tilde{T}_1, \dots, \tilde{T}_m$  is asymptotically jointly Gaussian and that the results of Benjamini and Yekutieli (2001) can be applied, but this is outside the scope of the present paper.

## 4 Results

In this section we quantify the effects of time and ENSO in the location parameter of the GEV and study their significance, using  $q = 0.05$  and  $q = 0.2$ , corresponding to control of the false discovery rate at the nominal levels 5% and 20%. In each case we first discuss PROD, which is the main variable of interest for severe thunderstorm risk, and then consider CAPE and SRH.

We begin with the effect of time. Table 2 shows that many of the 651 grid points exhibit a significant time trend for PROD in April, May and August (and to a lesser extent in June and December). In April, this number equals 313 at the 20% level, so (5)

implies that at least 250 of these grid points indeed have a trend; with (6), this number rises to 278. Figure 6 indicates that, in April, the North-East, a very wide South-East corner and the South-West, show significant time trends. In the first two regions,  $\hat{\eta}_{1,ti}$  is positive, corresponding to an increasing risk of severe thunderstorms, particularly in already risky parts of the US. Similar conclusions may be drawn from Figure 7 in the case of May, though the South-East is less prominent.

Regarding CAPE, April, May and June (and to a lesser extent August, November and January) show many grid points with a significant time trend. For April and May, Figures 6 and 7 show significantly negative  $\hat{\eta}_{1,ti}$  in the West, contrasting with a significantly positive trend in the center and the East. As pointed out by Trapp et al. (2009) and Diffenbaugh et al. (2013), a positive time trend for CAPE is expected in a context of climate change. However, to the best of our knowledge, such a trend has not previously been observed in the literature.

For SRH, May and to a lesser extent April have many significantly positive grid points spread approximately uniformly except in a large South-West corner in April and a large South-East corner in May. The significance for PROD in April and May comes from both CAPE and SRH. Figures 6 and 7 suggest that the significant positive time trend in the “most” risky part of the US stems mainly from CAPE in April and mainly from SRH in May.

We now comment on the effect of ENSO. For PROD, Table 2 reveals that many grid points exhibit a significant relation in February. Figure 8 indicates that  $\hat{\eta}_{1,en}$  is negative at those and that the main regions concerned are the North-East, the South-Center and the North-West; we expect higher PROD maxima during La Niña years in these regions.

Regarding CAPE, there is no striking result in terms of significance.

For SRH, a very large number of grid points exhibit significance in February. Figure 8 shows that almost all grid points are concerned except for a strip in the North and a tiny diagonal strip in the South-East corner of the region. The estimate  $\hat{\eta}_{1,en}$  is highly negative in most of the region but very positive in the extreme South-East, with a very rapid change in sign, presumably due to proximity with the Gulf of Mexico. There is a significant negative relation in regions at risk of thunderstorms or large-scale storms, for which SRH plays an essential role. This risk may increase during La Niña years. A relationship between monthly averages of SRH and ENSO for winter months was noticed by Allen et al. (2015). Finally, Figure 8 suggests that CAPE contributes more to PROD than SRH in terms of significance, although the relation with ENSO is more pronounced for SRH than for CAPE.

| Variable         | Covariate   | q    | Jan | Feb | Mar | Apr | May | Jun | Jul | Aug | Sep | Oct | Nov | Dec |
|------------------|-------------|------|-----|-----|-----|-----|-----|-----|-----|-----|-----|-----|-----|-----|
| <b>PROD</b>      | <b>Time</b> | 0.05 | 7   | 0   | 1   | 41  | 36  | 0   | 0   | 36  | 2   | 0   | 0   | 22  |
|                  | <b>Time</b> | 0.2  | 40  | 0   | 4   | 313 | 203 | 81  | 13  | 148 | 23  | 0   | 0   | 98  |
|                  | <b>ENSO</b> | 0.05 | 0   | 58  | 10  | 0   | 0   | 1   | 0   | 0   | 0   | 0   | 0   | 1   |
|                  | <b>ENSO</b> | 0.2  | 1   | 172 | 26  | 0   | 3   | 3   | 0   | 0   | 0   | 0   | 0   | 1   |
| <b>CAPE</b>      | <b>Time</b> | 0.05 | 37  | 13  | 28  | 109 | 60  | 89  | 18  | 55  | 4   | 0   | 30  | 1   |
|                  | <b>Time</b> | 0.2  | 92  | 37  | 73  | 268 | 273 | 206 | 75  | 133 | 35  | 40  | 134 | 16  |
|                  | <b>ENSO</b> | 0.05 | 15  | 0   | 0   | 0   | 0   | 2   | 2   | 0   | 0   | 0   | 1   | 1   |
|                  | <b>ENSO</b> | 0.2  | 27  | 11  | 21  | 0   | 0   | 3   | 16  | 14  | 0   | 1   | 6   | 13  |
| <b>SRH</b>       | <b>Time</b> | 0.05 | 0   | 1   | 0   | 7   | 43  | 2   | 1   | 7   | 0   | 0   | 0   | 0   |
|                  | <b>Time</b> | 0.2  | 15  | 44  | 4   | 138 | 230 | 14  | 50  | 45  | 6   | 0   | 0   | 27  |
|                  | <b>ENSO</b> | 0.05 | 0   | 255 | 0   | 0   | 1   | 0   | 0   | 0   | 0   | 0   | 0   | 0   |
|                  | <b>ENSO</b> | 0.2  | 3   | 384 | 59  | 18  | 4   | 0   | 8   | 7   | 4   | 1   | 0   | 82  |
| <b>PROD res.</b> | <b>Time</b> | 0.05 | 7   | 0   | 2   | 30  | 88  | 0   | 0   | 41  | 2   | 0   | 0   | 38  |
|                  | <b>Time</b> | 0.2  | 50  | 16  | 6   | 274 | 221 | 86  | 21  | 137 | 18  | 0   | 2   | 100 |
| <b>CAPE res.</b> | <b>Time</b> | 0.05 | 35  | 20  | 15  | 87  | 96  | 89  | 25  | 59  | 9   | 0   | 19  | 2   |
|                  | <b>Time</b> | 0.2  | 88  | 46  | 51  | 219 | 267 | 223 | 91  | 139 | 54  | 41  | 120 | 29  |
| <b>SRH res.</b>  | <b>Time</b> | 0.05 | 0   | 0   | 0   | 7   | 38  | 2   | 1   | 7   | 0   | 0   | 0   | 0   |
|                  | <b>Time</b> | 0.2  | 20  | 1   | 6   | 126 | 241 | 7   | 46  | 41  | 1   | 0   | 0   | 60  |
| <b>PROD res.</b> | <b>ENSO</b> | 0.05 | 1   | 66  | 8   | 0   | 0   | 1   | 0   | 0   | 0   | 0   | 0   | 7   |
|                  | <b>ENSO</b> | 0.2  | 1   | 178 | 26  | 0   | 49  | 3   | 0   | 0   | 0   | 0   | 0   | 33  |
| <b>CAPE res.</b> | <b>ENSO</b> | 0.05 | 1   | 0   | 0   | 0   | 0   | 3   | 5   | 1   | 0   | 0   | 0   | 2   |
|                  | <b>ENSO</b> | 0.2  | 21  | 38  | 0   | 1   | 0   | 4   | 17  | 16  | 0   | 0   | 1   | 21  |
| <b>SRH res.</b>  | <b>ENSO</b> | 0.05 | 0   | 209 | 0   | 0   | 4   | 0   | 0   | 0   | 1   | 0   | 0   | 0   |
|                  | <b>ENSO</b> | 0.2  | 1   | 359 | 20  | 38  | 14  | 0   | 3   | 7   | 2   | 1   | 0   | 63  |

Table 2: Number of grid points where  $\hat{\eta}_{1,ti}$  and  $\hat{\eta}_{1,en}$  are significant for PROD, CAPE and SRH maxima for each month (top); number of grid points where  $\hat{\eta}_{1,ti}$  is significant for PROD, CAPE and SRH maxima residuals after accounting for the relation with ENSO (middle); number of grid points where  $\hat{\eta}_{1,en}$  is significant for PROD, CAPE and SRH maxima residuals after accounting for the relation with time (bottom). We have accounted for multiple testing using the BH procedure with the values of  $q$  displayed.

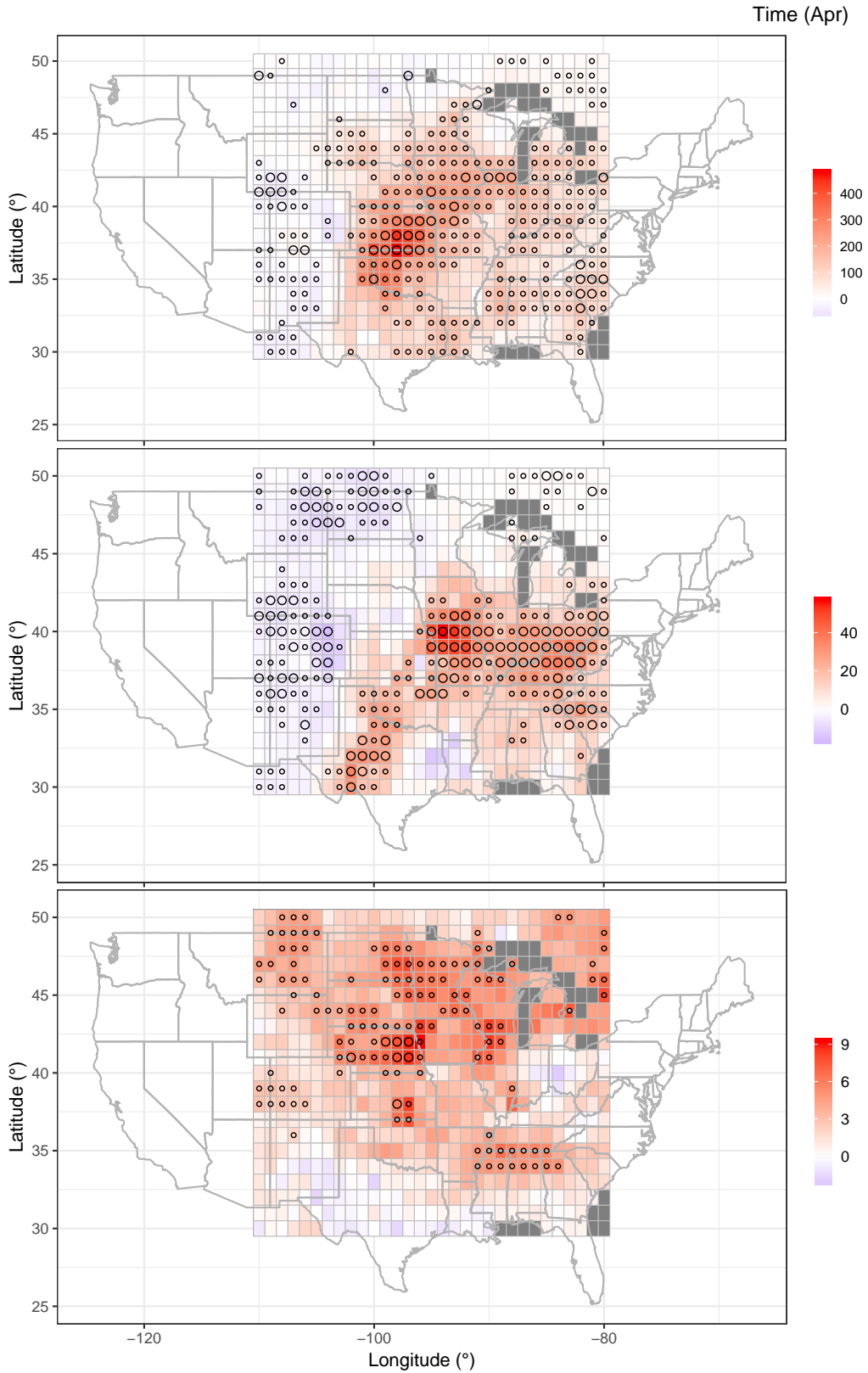


Figure 6: Values and significance of the slope  $\hat{\eta}_{1,t_i}$  for PROD (top), CAPE (middle) and SRH (bottom) maxima in April. Large and small circles indicate significance (after accounting for multiple testing using the BH procedure) at any level not lower than 5% and 20%, respectively. The units of  $\hat{\eta}_{1,t_i}$  are  $\text{m}^3\text{s}^{-3}\text{yr}^{-1}$ ,  $\text{Jkg}^{-1}\text{yr}^{-1}$  and  $\text{m}^2\text{s}^{-2}\text{yr}^{-1}$  for PROD, CAPE and SRH, respectively. Dark grey corresponds to grid points where no observations are available.

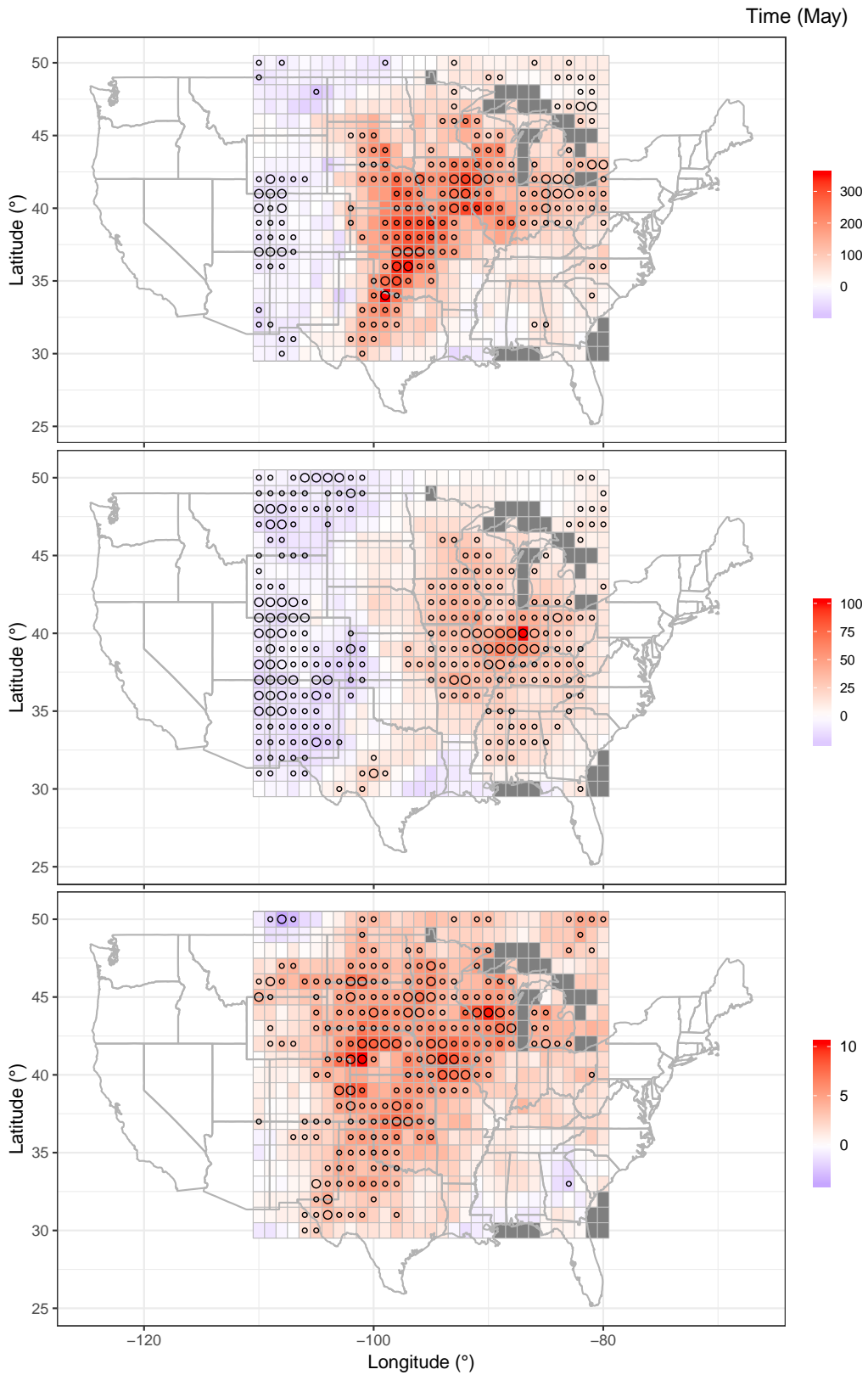


Figure 7: Same content as in Figure 6 in the case of May.

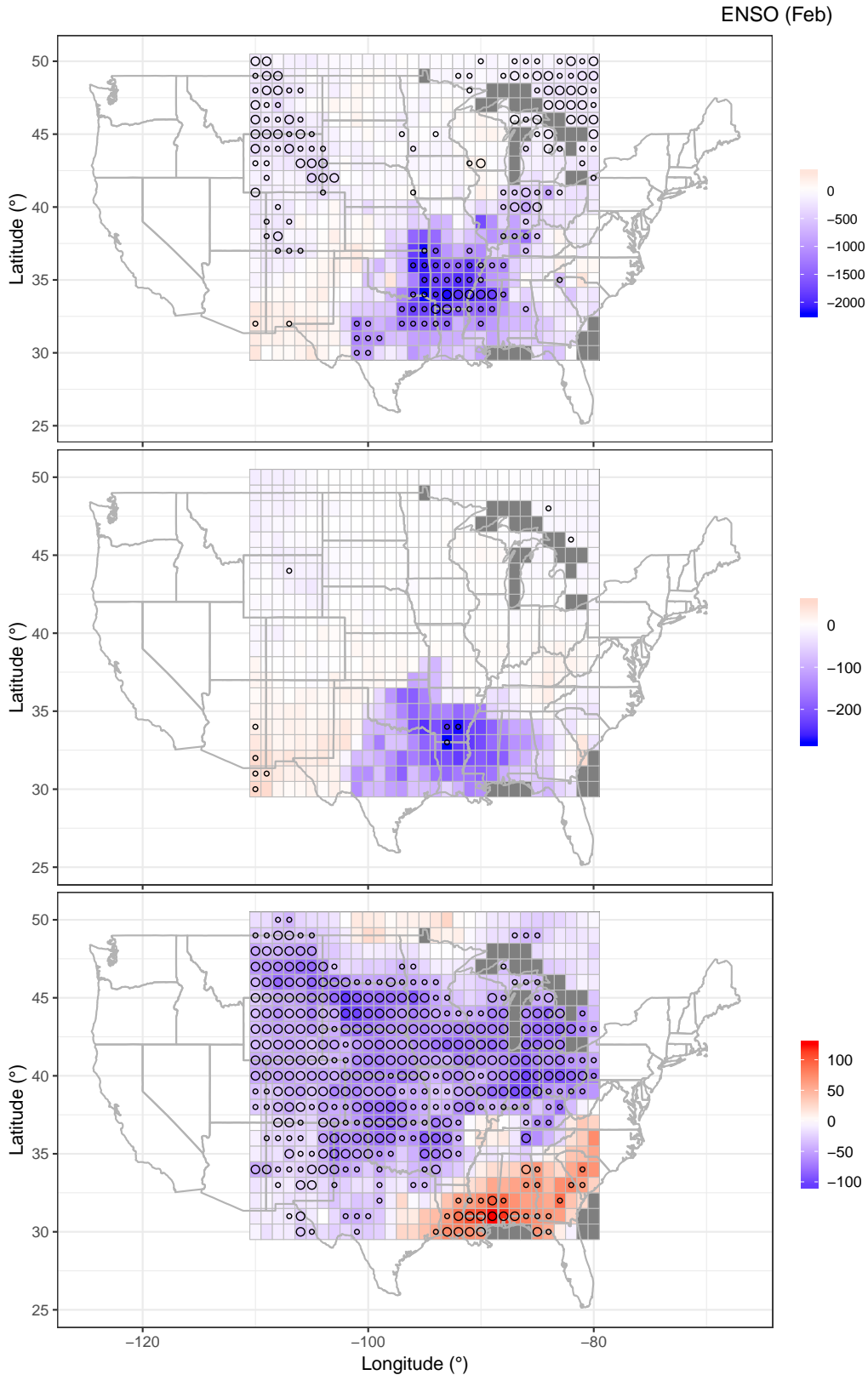


Figure 8: Values and significance of  $\hat{\eta}_{1,en}$  for PROD (top), CAPE (middle) and SRH (bottom) maxima in February. Large and small circles indicate significance (after accounting for multiple testing using the BH procedure) at any level not lower than 5% and 20%, respectively. The units of  $\hat{\eta}_{1,en}$  are  $\text{m}^3\text{s}^{-3}\text{C}^{-1}$ ,  $\text{Jkg}^{-1}\text{C}^{-1}$  and  $\text{m}^2\text{s}^{-2}\text{C}^{-1}$  for PROD, CAPE and SRH, respectively.

We also considered the residuals of PROD, CAPE and SRH maxima after accounting for ENSO or temporal effects. For instance, if we observe a time trend, the idea of considering the residuals after accounting for ENSO is to determine whether the time trend is explained by ENSO. This allows us to determine whether the time and ENSO effects are “independent”.

In the case of PROD, Table 2 shows that removing ENSO does not much decrease the number of grid points exhibiting a significant time trend; there is a slight decrease for April but a small increase for some other months. Accounting for the time trend, on the other hand, can slightly increase the number of grid points showing a significant relation with ENSO. For CAPE, removing ENSO decreases the number of grid points exhibiting a significant time trend for March, but there is a slight increase for other months, whereas accounting for time slightly decreases the number of grid points showing a significant relation with ENSO in January and March only, with a slight increase in other months. Regarding SRH, removing ENSO decreases the number of grid points exhibiting a significant time trend in February but there is little impact for other months. The conclusions are similar when accounting for the time trend and studying the ENSO effect. The maps of the residuals, available upon request, show that when removing a covariate has little impact on the number of grid points at which the relation with the other covariate is significant, it has almost no impact on their locations neither. To summarize, the effects of time and ENSO appear “independent”, except for CAPE in January and March and SRH in February.

## 5 Conclusion

In this study, we quantify the effects of time and ENSO on the distribution of monthly maxima of PROD, CAPE and SRH, which are highly relevant to the risk of severe thunderstorms. We demonstrate that the use of the GEV is justified in our setting. Using an appropriate treatment of multiple testing, we point out the existence of a significant time trend in the location parameter of the GEV for PROD maxima in April, May and August, CAPE maxima in April, May and June and SRH maxima in April and May. The latter months are prominent for PROD, as severe thunderstorms are recurrent at this period. The corresponding time slope is positive in parts of the US where the risk was already high, which may have important consequences. We also found ENSO to be a good covariate in the location parameter of the GEV for PROD and SRH maxima in February. The corresponding relationship for SRH is negative over most of the region we consider, perhaps implying that storm risk increases in February during La Niña years.

## Acknowledgements

The two first authors contributed equally to this paper. The work was supported the Swiss National Science Foundation (project number 200021\_178824).



## References

- Agee, E., Larson, J., Childs, S., and Marmo, A. (2016). Spatial redistribution of USA tornado activity between 1954 and 2013. *J. Appl. Meteor. Climatol.*, 55:1681–1697.
- Allen, J. T. and Tippett, M. K. (2015). The characteristics of United States hail reports: 1955-2014. *Electronic J. Severe Storms Meteor.*, 10:1–31.
- Allen, J. T., Tippett, M. K., and Sobel, A. H. (2015). Influence of the El Niño/Southern Oscillation on tornado and hail frequency in the United States. *Nat. Geosci.*, 8:278–283.
- Benjamini, Y. and Hochberg, Y. (1995). Controlling the false discovery rate: a practical and powerful approach to multiple testing. *Journal of the Royal Statistical Society. Series B (Methodological)*, 57(1):289–300.
- Benjamini, Y. and Yekutieli, D. (2001). The control of the false discovery rate in multiple testing under dependency. *The Annals of Statistics*, 29(4):1165–1188.
- Brooks, H. E. (2013). Severe thunderstorms and climate change. *Atmospheric Research*, 123:129–138.
- Brooks, H. E., Carbin, G. W., and Marsh, P. T. (2014). Increased variability of tornado occurrence in the United States. *Science*, 346:349–352.
- Brooks, H. E., Lee, J. W., and Craven, J. P. (2003). The spatial distribution of severe thunderstorm and tornado environments from global reanalysis data. *Atmos. Res.*, 67-68:73–94.
- Coles, S. G. (2001). *An Introduction to Statistical Modeling of Extreme Values*. Springer, New York.
- Davies, J. M., Johns, R. H., and Leftwich, P. W. (1993). *The Tornado: Its Structure, Dynamics, Prediction, and Hazards*, chapter Some wind and instability parameters associated with strong and violent tornadoes. 2. Variations in the combinations of wind and instability parameters., pages 573–582. Number 79 in Geophys. Monogr. Amer. Geophys. Union.
- Davison, A. C. and Huser, R. (2015). Statistics of extremes. *Annual Review of Statistics and its Application*, 2:203–235.
- DelSole, T. and Yang, X. (2011). Field significance of regression patterns. *Journal of Climate*, 24(19):5094–5107.
- Diffenbaugh, N. S., Scherer, M., and Trapp, R. J. (2013). Robust increases in severe thunderstorm environments in response to greenhouse forcing. *Proc. Natl. Acad. Sci. (USA)*, 110:16361–16366.
- Doswell, III, C. A., Brooks, H. E., and Maddox, R. A. (1996). Flash flood forecasting: An ingredients-based methodology. *Wea. Forecasting*, 11:560–581.
- Edwards, R., Allen, J. T., and Carbin, G. W. (2018). Reliability and climatological impacts of convective wind estimations. *J. Appl. Meteor. Climatol.*, 57:1825–1845.

- Elsner, J. B., Elsner, S. C., and Jagger, T. H. (2015). The increasing efficiency of tornado days in the United States. *Clim. Dyn.*, 45:651–659.
- Embrechts, P., Mikosch, T., and Klüppelberg, C. (1997). *Modelling Extremal Events for Insurance and Finance*. Springer-Verlag Berlin Heidelberg.
- Gensini, V. A. and Brooks, H. E. (2018). Spatial trends in united states tornado frequency. *npj Climate and Atmospheric Science*, 1:38.
- Gilleland, E., Pocerlich, M., Brooks, H. E., Brown, B. G., and Marsh, P. (2008). Large-scale indicators for severe weather. *Manuscript in Preparation*.
- Lepore, C., Tippett, M. K., and Allen, J. T. (2017). ENSO-based probabilistic forecasts of March-May U.S. tornado and hail activity. *Geophys. Res. Lett.*, 44:9093–9101.
- Livezey, R. E. and Chen, W. Y. (1983). Statistical field significance and its determination by Monte Carlo techniques. *Monthly Weather Review*, 111(1):46–59.
- Mannshardt, E. and Gilleland, E. (2013). Extremes of severe storm environments under a changing climate. *American Journal of Climate Change*, 2(3A):47–61.
- Mesinger, F. and Coauthors (2006). North American Regional Reanalysis. *Bull. Amer. Meteor. Soc.*, 87:343–360.
- Rasmussen, E. N. and Blanchard, D. O. (1998). A baseline climatology of sounding-derived supercell and tornado forecast parameters. *Wea. Forecasting*, 13:1148–1164.
- Tippett, M. K., Lepore, C., and Cohen, J. E. (2016). More tornadoes in the most extreme U.S. tornado outbreaks. *Science*, 354:1419–1423.
- Trapp, R. J., Diefenbaugh, N. S., and Gluhovsky, A. (2009). Transient response of severe thunderstorm forcing to elevated greenhouse gas concentrations. *Geophys. Res. Lett.*, 36:L01703.
- Ventura, V., Paciorek, C. J., and Risbey, J. S. (2004). Controlling the proportion of falsely rejected hypotheses when conducting multiple tests with climatological data. *Journal of Climate*, 17(22):4343–4356.
- Verbout, S. M., Brooks, H. E., Leslie, L. M., and Schultz, D. M. (2006). Evolution of the U.S. tornado database: 1954-2003. *Wea. Forecasting*, 21:86–93.
- Yekutieli, D. and Benjamini, Y. (1999). Resampling-based false discovery rate controlling multiple test procedures for correlated test statistics. *Journal of Statistical Planning and Inference*, 82(1-2):171–196.